Hindawi
International Journal of Aerospace Engineering
Volume 2020, Article ID 8896744, 14 pages
https://doi.org/10.1155/2020/8896744

Research Article

Passive Suppression of Panel Flutter Using a Nonlinear Energy Sink

Jian Zhou, Minglong Xu, and Wei Xia

State Key Laboratory for Strength and Vibration of Mechanical Structures, School of Aerospace Engineering, Xi'an Jiaotong University, Xi'an, China

Correspondence should be addressed to Jian Zhou; zhoujian1986315@163.com

Received 6 April 2020; Revised 17 June 2020; Accepted 23 June 2020; Published 11 July 2020

Academic Editor: Mohammad Tawfik

A nonlinear energy sink (NES) is used to suppress panel flutter. A nonlinear aeroelastic model for a two-dimensional flat panel with an NES in supersonic flow is established using the Galerkin method. First-order piston aerodynamic theory is adopted to build the aerodynamic load. The effects of NES parameters on flutter boundaries of the panel are investigated using Lyapunov's indirect method. The mechanism of the NES suppression of panel flutter is studied through energy analysis. Effects of NES parameters on aeroelastic responses of the panel are obtained, and a design technique is adopted to find a suitable combination of parameter values of the NES that suppresses the panel flutter effectively. Results show that the NES can increase or reduce the onset dynamic pressure of the panel flutter and it can reduce the aeroelastic response amplitude effectively within a certain range of dynamic pressure behind the onset dynamic pressure. The installation position of the NES depends on the direction of the airflow. The robust characteristics should be considered to find the suitable combination of parameter values of the NES.

1. Introduction

Panel flutter, which is a type of dynamic aeroelastic instability resulting from the interaction of aerodynamic, inertial, and elastic forces, can be described as a self-excited oscillation of the external skin panel of a flight vehicle with one side exposed to, usually, supersonic or hypersonic airflow. There have been some accidents resulting from panel flutter since flight vehicles reached supersonic speeds in the 1950s [1]. Consequently, panel flutter problems have been widely studied by aeroelastic researchers for decades [2–6]. Because of the geometric nonlinearity of panel vibration, panel flutter usually exhibits limited amplitude vibration, which can lead to fatigue failure, rather than divergent vibration. Different strategies [7–11], including active and passive controls, have thus been proposed to increase the onset dynamic pressure of the panel or suppress the aeroelastic amplitude. While active control has been shown to be effective in suppressing structural vibration, however, this method requires external actuators and sensors. There are no such requirements in passive vibration control, which is inherently robust and simple to implement.

This work proposes a passive control strategy, namely, the use of a nonlinear energy sink (NES), to suppress panel flutter or reduce the aeroelastic response of the panel. The NES comprises a small mass, a linear damper, and a nonlinear spring and is attached to the panel at a predetermined position. Unlike the linear dynamic absorber, which is effective only in a narrow frequency band, the NES is effective within a broadband range of frequencies [12] owing to the nonlinear stiffness of the NES. The NES has mostly been studied in discrete vibration systems of coupled oscillators [13–16]. Georgiades and Vakakis [17] first attached the NES to a continuous primary vibration system (a linear beam structure) and proposed that the NES could be applied to the suppression of structural dynamic instabilities, such as limit cycle oscillations and flutter. Since then, the NES had been applied to suppress the vibration of many structures, includ-

ing rods [18], beams [19, 20], plates [21, 22] and fluid-conveying pipes [23]. Recently, Lee et al. [24] demonstrated that the NES can improve the stability of the aeroelastic system of a two-dimensional (2D) wing by experiments and theoretical analysis. Bichiou et al. [25] demonstrated the effectiveness of the NES in controlling the flutter of a 2D wing and realized the beneficial effect of the NES in reducing the pitch and plunge amplitude; however, this reduction is limited to a small region of free-stream velocities above the flutter speed. Ebrahimzade et al. [26] investigated the performance of linear passive vibration absorbers and the NES on the stability properties and nonlinear behaviors of an aeroelastic system. Yan et al. [27] evaluated the usability of the NES in controlling the nonlinear transonic flutter of a 2D wing aeroelastic system and showed that the NES may shift the wing flutter system to a new equilibrium position, in terms of the mean oscillation. Zhang et al. [28] studied the airflow-induced vibration of a 2D wing coupled with two nonlinear energy sinks in a free stream and analyzed the relationship between vibration suppression and targeted energy transfer.

Meanwhile, researchers also have applied the NES to suppress panel flutter. Zhang et al. [29] applied the NES to a flat panel aeroelastic system; however, they only investigated the preflutter responses and showed that the NES can reduce the vibration amplitude of the plate quickly. Pacheco et al. [30] provided important insights into the mechanism through which an NES can suppress the panel flutter response. However, only a few discrete dynamic pressures were used to illustrate the effectiveness of panel flutter suppression, and some unique nonlinear behaviors, such as the phenomenon of transient resonance capture, were not obtained for the panel-NES aeroelastic system.

The present work investigates the efficiency and mechanism of the suppression of the panel flutter by an NES using a 2D aeroelastic flat panel system. The governing equations for a 2D flat panel with an NES in supersonic air flow are established in Section 2. Stability analysis is performed in Section 3 to investigate the effects of NES parameters on the panel flutter boundary. Nonlinear aeroelastic behaviors are performed in Section 4 to investigate the efficiency and mechanism of panel flutter suppression using the NES. The effects of NES parameters on the bifurcation performance of a coupled aeroelastic panel system are obtained, and a technique of designing NES parameters is adopted in Section 5. Conclusions are presented in Section 6.

2. Governing Equations

Similar to the study of wing aeroelasticity, the aeroelastic flat panel model can be simplified to a 2D flat panel in a mechanism study [6]. Figure 1 is a schematic diagram of an aeroelastic model of a 2D flat panel with an NES. x and z are, respectively, horizontal and vertical coordinates. The system comprises a 2D isotropic panel with simply supported boundary conditions and a nonlinear energy sink with pure cubic stiffness nonlinearity installed on the panel. The requirement of pure cubic stiffness nonlinearity of the NES plays a key role in the realization of targeted energy transfer,

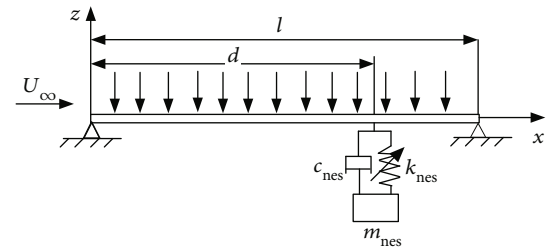

Figure 1: A 2D aeroelastic flat panel model coupled with an NES.

since it precludes the existence of a preferential resonance frequency for the NES.

The governing equations for a 2D flat panel in supersonic airflow can be obtained from the literature [31]. On the basis of the modeling of a hybrid vibration system [32], the governing equations for a 2D aeroelastic flat panel with an NES in supersonic air flow can be written as

$$\rho h\ddot{w} + c\dot{w} - N_p w_{xx} + Dw_{xxxx} + \left\{k_{nes}[w(x,t) - v]^3 + c_{nes}[\dot{w}(x,t) - \dot{v}]\right\}\delta(x-d) = P - P_\infty, \tag{1}$$

$$m_{nes}\ddot{v} + k_{nes}[v - w(d,t)]^3 + c_{nes}[\dot{v} - \dot{w}(d,t)] = 0, \tag{2}$$

where a dot denotes differentiation with respect to time t, while the subscript x represents partial differentiation with respect to x; c is the damping parameter; $N_p = (Eh/2l)\int_0^l w_x^2\,dx$ is the in-plane load; $D = Eh^3/12(1-\upsilon^2)$ is the bending stiffness of the panel; E is Young's modulus; l is the length of the panel; υ is Poisson's ratio; ρ and h are, respectively, the density and thickness of the panel; P and P_∞ are, respectively, the aerodynamic pressures on the upper and lower surfaces of the panel; w is the vibration deflection of the panel and v is the displacement of the NES; d, k_{nes}, c_{nes}, and m_{nes} are, respectively, the installation position, nonlinear stiffness coefficient, damping, and mass of the NES; and $\delta(x-d)$ is the Dirac function, having a dimension of l^{-1}.

First-order piston theory aerodynamics is sufficient to simulate the aerodynamic load acting on the panel surface [5, 6]:

$$P - P_\infty = -\frac{2q}{\beta}\left(w_x + \frac{\mathrm{Ma}^2 - 2}{\mathrm{Ma}^2 - 1}\frac{1}{U_\infty}\dot{w}\right), \tag{3}$$

where $q = \rho_\infty U_\infty^2/2$ is the dynamic pressure; ρ_∞ and U_∞ are, respectively, the density and speed of undisturbed air flow; $\beta = \sqrt{\mathrm{Ma}^2 - 1}$ is the Prandtl-Glauert factor; and Ma is the Mach number.

Equations (1) and (2) are expressed in nondimensional form by defining nondimensional variables

$$\begin{aligned}
\xi &= \frac{x}{l}, \\
\bar{d} &= \frac{d}{l}, \\
W &= \frac{w}{h}, \\
V &= \frac{v}{h}, \\
\tau &= t\sqrt{\frac{D}{\rho h l^4}}, \\
\mu &= \frac{\rho_\infty l}{\rho h}, \\
\lambda &= \frac{2ql^3}{\beta D}, \\
M_{\text{nes}} &= \frac{m_{\text{nes}}}{\rho h l}, \\
K_{\text{nes}} &= \frac{k_{\text{nes}} h^2 l^3}{D}, \\
C &= c\sqrt{\frac{l^4}{\rho h D}}, \\
C_{\text{nes}} &= c_{\text{nes}}\sqrt{\frac{l^2}{\rho h D}}, \\
R_M &= \left(\frac{\text{Ma}^2 - 2}{\text{Ma}^2 - 1}\right)\frac{\mu}{\beta}.
\end{aligned} \tag{4}$$

Introducing these nondimensional variables into the coupled aeroelastic panel system of Equations (1) and (2) gives the dimensionless equations

$$\begin{aligned}
&\ddot{W} + C\dot{W} - 6\left(1\text{-}\upsilon^2\right) W_{\xi\xi}\int_0^1 W_\xi^2 d\xi + W_{\xi\xi\xi\xi} + \lambda W_\xi + \sqrt{\lambda R_M}\dot{W} \\
&\quad + \left\{K_{\text{nes}}\left[W(\xi,\tau) - V\right]^3 + C_{\text{nes}}\left[\dot{W}(\xi,\tau) - \dot{V}\right]\right\}\delta\left(\xi - \bar{d}\right) = 0,
\end{aligned} \tag{5}$$

$$M_{\text{nes}}\ddot{V} + K_{\text{nes}}\left[V - W\left(\bar{d},\tau\right)\right]^3 + C_{\text{nes}}\left[\dot{V} - \dot{W}\left(\bar{d},\tau\right)\right] = 0. \tag{6}$$

The Galerkin method is used to discretize the above motion equations. The displacement of the panel can be expressed as a series of assumed modes:

$$W(\xi,\tau) = \sum_{m=1}^{N} a_m(\tau)\,\sin m\pi\xi. \tag{7}$$

Substitute Equation (7) into Equations (5) and (6), and then multiply each term of Equation (5) by $\sin s\pi\xi$ and integrating over the panel length. A set of coupled ordinary nonlinear differential equations can be obtained.

$$\begin{aligned}
&\ddot{a}_s + C\dot{a}_s + 6\left(1\text{-}\upsilon^2\right)\left[\sum_{r=1}^{N} a_r^2\frac{(r\pi)^2}{2}\right]a_s(s\pi)^2 + a_s(s\pi)^4 \\
&\quad + \lambda\sum_{\substack{m=1,\\ m\neq s}}^{N}\frac{2sm}{s^2 - m^2}\left[1 - (-1)^{s+m}\right]a_m + \sqrt{\lambda R_M}\dot{a}_s \\
&\quad + 2\left[K_{\text{nes}}\left(\sum_{m=1}^{N} a_m\,\sin m\pi\bar{d} - V\right)^3\right. \\
&\quad \left. + C_{\text{nes}}\left(\sum_{m=1}^{N}\dot{a}_m\,\sin m\pi\bar{d} - \dot{V}\right)\right]\sin s\pi\bar{d} = 0, \\
&M_{\text{nes}}\ddot{V} + K_{\text{nes}}\left(V - \sum_{m=1}^{N} a_m\,\sin m\pi\bar{d}\right)^3 \\
&\quad + C_{\text{nes}}\left(\dot{V} - \sum_{m=1}^{N}\dot{a}_m\,\sin m\pi\bar{d}\right) = 0, \\
&s = 1, 2, \cdots, N.
\end{aligned} \tag{8}$$

The study of energy transfer between the panel and NES requires the evaluation of quantities such as the mechanical energy and the power dissipation/input. The transient energy of the panel and the NES should be first defined.

The transient kinetic energy of the panel is

$$\text{EK}_\text{p} = \frac{1}{2}\rho h\int_0^l \dot{w}^2 dx. \tag{9}$$

The transient potential energy of the panel is

$$\text{EP}_\text{p} = \frac{1}{2}\iiint_V \sigma_x\varepsilon_x dV = \frac{1}{24}Eh^3\int_0^l w_{xx}^2 dx + \frac{1}{8}Eh\int_0^l w_x^4 dx, \tag{10}$$

where $\sigma_x = E\varepsilon_x$ denotes the stress components corresponding to the in-plane strains and $\varepsilon_x = -zw_{xx} + w_x^2/2$ is the in-plane strain induced by the out-of-plane displacement.

The transient kinetic energy of the NES is

$$\text{EK}_\text{n} = \frac{1}{2}m_{\text{nes}}\dot{v}^2. \tag{11}$$

The transient potential energy of the NES is

$$\text{EP}_\text{n} = \frac{1}{4}k_{\text{nes}}[w(d,t) - v]^4. \tag{12}$$

The input energy provided by the air flow before time t is

$$\text{EF} = \int_0^t\int_0^l (P - P_\infty)\dot{w}\,dx\,dt. \tag{13}$$

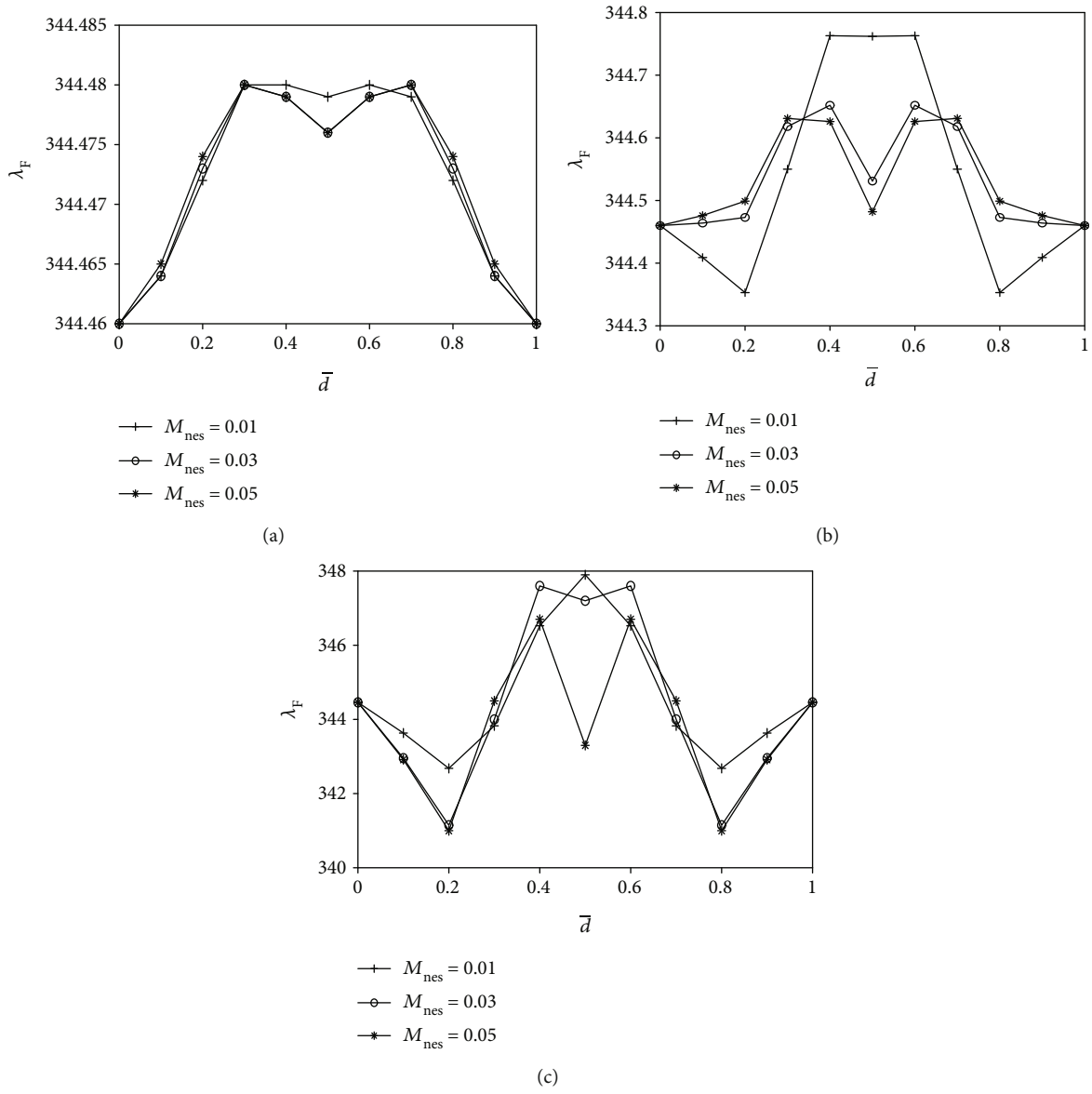

Figure 2: Effects of M_{nes} and $\bar{d}$ on the stability boundaries for different damping coefficients: (a) $C_{nes} = 0.01$, (b) $C_{nes} = 0.1$, and (c) $C_{nes} = 1$.

The total input energy is the sum of the initial energy provided by the initial conditions and the work done by the air flow:

$$\mathrm{EI} = E_0 + \mathrm{EF}. \tag{14}$$

The total energy dissipated by the panel and NES before time $t$is

$$\mathrm{ED} = \int_0^t \left\{ c \int_0^l \dot{w}^2 dx + c_{nes}[\dot{w}(d,t) - \dot{v}]^2 \right\} dt. \tag{15}$$

The total transient energy of the panel is

$$\mathrm{ET_p} = \mathrm{EK_p} + \mathrm{EP_p}. \tag{16}$$

The total transient energy of the NES is

$$\mathrm{ET_n} = \mathrm{EK_n} + \mathrm{EP_n}. \tag{17}$$

In this study, the parameters of the panel are chosen as [33] follows: $l = 0.5$ m, $h = 0.002$ m, $E = 78.55$ GPa, $\rho = 2710$ kg/m^3, and $\upsilon = 0.3$. The Mach number and sound speed of the air flow are, respectively Ma = 2.0 and $a = 295.065$ m/s.

3. Stability Analysis

Transforming the equations of motion into the state space, the flutter boundary of the aeroelastic panel can be obtained using Lyapunov's indirect method. The system variables

a_i, V comprise static equilibrium solutions $\widehat{a}_i$, $\widehat{V}$ and small perturbationsε_i, ε_{2N+1}:

$$\begin{aligned} a_i &= \widehat{a}_i + \varepsilon_i, \\ a_{N+i} &= \varepsilon_{N+i}, \\ V &= \widehat{V} + \varepsilon_{2N+1}, \\ \dot{V} &= \varepsilon_{2N+2}, \\ i &= 1, 2, \cdots, N. \end{aligned} \tag{18}$$

In the neighborhood of the static equilibrium solutions, the state-space equations can be linearized as

$$\dot{\boldsymbol{\varepsilon}} = A\boldsymbol{\varepsilon}, \tag{19}$$

where $\boldsymbol{\varepsilon} = [\varepsilon_1\ \varepsilon_2\ \cdots\ \varepsilon_{2N+2}]^T$ and A is the Jacobi matrix of the panel system at $a_i = \widehat{a}_i$ and $V = \widehat{V}$. For a flat panel, $\widehat{a}_i = 0$ and $\widehat{V} = 0$.

Assuming $\varepsilon_i = \varepsilon_{i0}e^{\Omega\tau}$, we get the eigenequation of Equation (19):

$$|A - \Omega I| = 0. \tag{20}$$

The complex eigenvalue is denoted $\Omega = \Omega_R \pm i\Omega_I$. The aeroelastic system of the panel with an NES is stable when $\Omega_R < 0$ and unstable when$\Omega_R > 0$. The flutter boundary of the panel with an NES is obtained at $\Omega_R = 0$ where the panel is undergoing harmonic motion.

Figure 2 shows the effect of the nondimensional mass M_{nes}, damping coefficients C_{nes}, and nondimensional installation position $\bar{d}$ on the stability boundaries of the panel with an NES. The stiffness term of the NES is a pure cubic stiffness term. When the state-space equations are linearized, the nonlinear stiffness coefficient K_{nes} is not included in the Jacobi matrix A for the plat panel, and the nonlinear stiffness coefficient thus does not affect the stability boundary of the panel with an NES. When $\bar{d} = 0$ or $\bar{d} = 1$, the critical dynamic pressure is 344.46, which represents the critical flutter dynamic pressure of the panel without an NES. It is noted that the stability boundary of the panel flutter with an NES is symmetrical on both sides of the central position, and the critical flutter dynamic pressure of the panel with an NES can be increased or reduced by changing the nondimensional mass, damping coefficient, and installation position of the NES. However, the effect of the NES on the stability boundaries of the panel is relatively small.

4. Nonlinear Aeroelastic Behaviors

This section investigates the nonlinear aeroelastic behaviors of the panel system with an NES, considering time responses and bifurcation diagrams, and studies the suppression mechanism by an energy-based analysis approach. The aeroelastic motion equations of the panel with an NES in the state space can be solved numerically by a fourth-order Runge-Kutta method, and the nonlinear aeroelastic response of the panel system with an NES can be obtained. Bifurcation diagrams

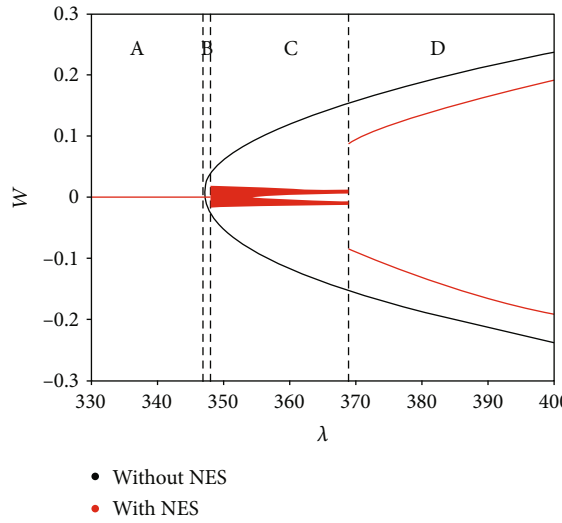

Figure 3: Bifurcation diagram of the panel flutter response with and without an NES.

are drawn by neglecting the transient response of the system, obtaining the peak and valley values of the steady-state response under a certain dynamic pressure, and then, continuously changing the dynamic pressure. The initial conditions and time step for time-domain response calculation are set at $W_0(\bar{d}) = 0.0005$, $\dot{W}_0(\bar{d}) = 0$, and $\Delta\tau = 0.001$. The bifurcation diagrams are drawn using response data at a position corresponding to 55% ($\xi = 0.55$) of the chord length.

Figure 3 shows a bifurcation diagram of the panel flutter response with and without an NES when $M_{\text{nes}} = 0.03$, $K_{\text{nes}} = 80000$, $C_{\text{nes}} = 0.3$, $C = 0.2$, and $\bar{d} = 0.55$. It is seen that the NES can reduce amplitudes of the nonlinear vibration responses effectively in a certain range of dynamic pressure above the onset dynamic pressure of the panel. According to the effect of the NES, the bifurcation diagram in Figure 3 can be divided into four regions: region A ($\lambda \le 346.8$), in which the response of the panel with or without an NES converges to the equilibrium position; region B ($346.8 < \lambda \le 348$), in which the response of the panel without an NES exhibits a stable limit cycle oscillation (LCO), but that of the panel with an NES converges to the equilibrium position; region C ($348 < \lambda \le 368.8$), in which the response of the panel without an NES exhibits a stable LCO, while that of the panel with an NES has a random-like vibration or a stable LCO with small amplitudes; and region D ($\lambda > 368.8$), in which the response of the panel with or without an NES exhibits a stable LCO. These four regions will be discussed in detail.

4.1. Region A. In region A, the response of the panel with or without an NES converges to an equilibrium position. Figure 4(a) compares the responses of the panel with and without an NES at dynamic pressure $\lambda = 346.8$. It is seen that the NES can drive the panel to the equilibrium position more quickly than that without an NES. Figure 4(b) depicts the responses of the panel and NES. It is seen that the response amplitudes of the NES are smaller than those of the panel, which illustrates that the targeted energy transfer does not

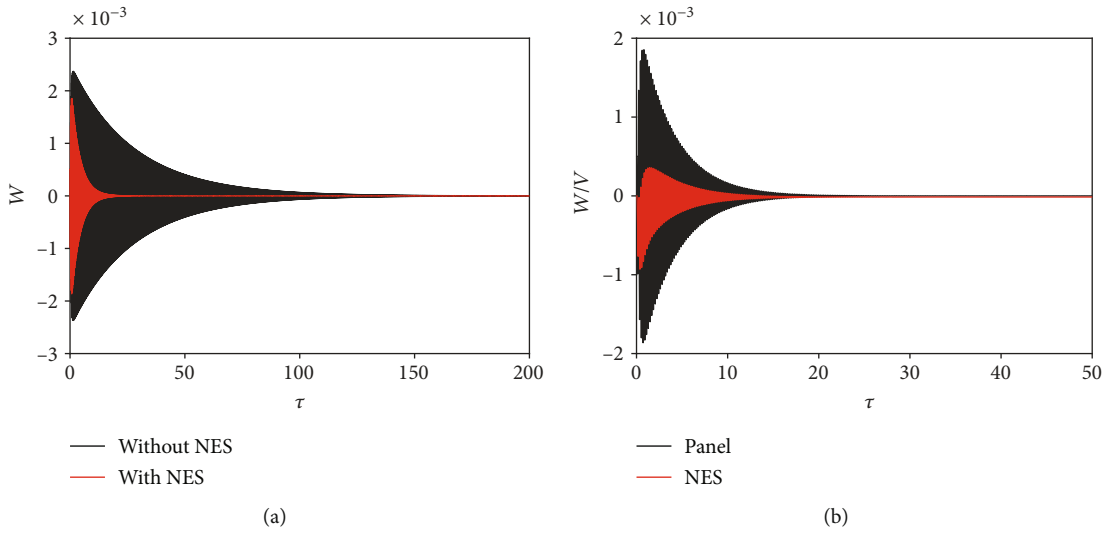

Figure 4: Time history at $\lambda = 346.8$: (a) responses of the panel with and without an NES; (b) responses of the NES and panel.

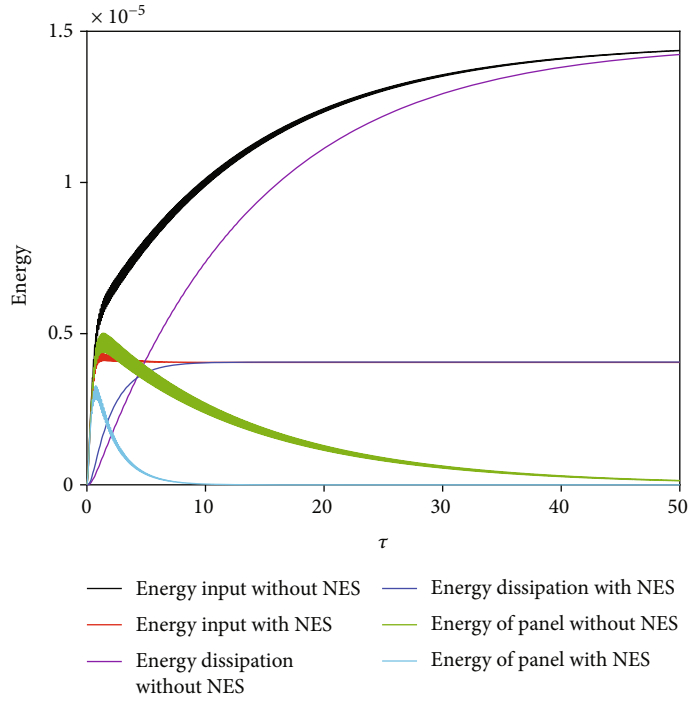

Figure 5: Time history of energy.

occur. This is because the vibration of the panel does not reach the vibration energy threshold at which the targeted energy transfer can occur [34].

The reason that the NES can quickly drive the panel to its equilibrium position can be explained by vibration energy analysis in Figure 5. The figure shows that the energy dissipated by the damping of the panel-NES system is obviously more than that dissipated by the damping of the panel without an NES in the initial stage. The net energy of the panel with an NES will be reduced, which will attenuate the vibration of the panel. Because panel flutter is a self-excited behavior, the input energy provided by airflow is then reduced due to the weakening of panel vibration. This is a continuous cycle process. Finally, the total energy input by airflow to the panel with an NES is less than that for the panel without an NES, and part of the input energy is dissipated by the damping of the NES while part is dissipated by the damping of the panel. The NES therefore drives the panel to the equilibrium position more rapidly.

4.2. Region B. In region B, the response of the panel without an NES exhibits a stable LCO while the response of panel with an NES converges to its equilibrium position as shown in Figure 6(a) at $\lambda = 348$. Section 3 revealed that the

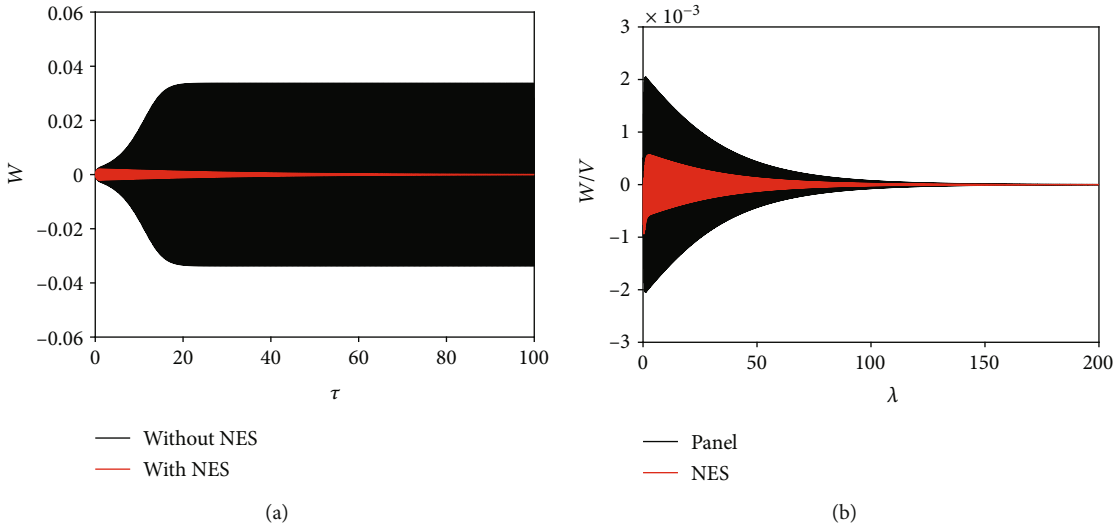

Figure 6: Time history at $\lambda = 348$: (a) responses of the panel with and without an NES; (b) responses of the NES and panel.

parameters such as the nondimensional mass, damping coefficient, and installation position of the NES affect the onset dynamic pressure of panel flutter. Region B therefore exists mainly owing to the parameters of the NES. Figure 6(b) shows the responses of the panel and the NES, which shows that the targeted energy transfer of the NES does not occur under this condition owing to the small vibration energy of the panel.

Vibration energy analysis is performed in Figure 7. Figure 7(a) shows that the energy dissipated by the panel without an NES is not sufficiently strong to offset the input energy from the airflow, which creates a difference between the energy input by airflow and the energy dissipated by the damping of the panel. This difference increases steadily with time and eventually reaches a balance (not zero). The panel finally exhibits a stable LCO. When the NES is attached to the panel, the vibration energy dissipated by the damping of the panel and the NES is more than that dissipated by the damping of the panel without an NES as shown in Figure 7(c), which can reduce the increasing rate of energy input by the airflow. As time passes, the increasing rate of energy input by the airflow becomes zero as shown in Figure 7(b). That is to say, there is no energy input from the airflow, and the panel then maintains an equilibrium position finally.

4.3. Region C. In region C, the nonlinear aeroelastic responses of the panel are completely suppressed, and the panel exhibits two types of nonlinear dynamic behaviors: a series of recurrent motion in Figure 8 at $\lambda = 355$ and a stable LCO with small amplitudes in Figure 9 at $\lambda = 368$. Figure 8(b) shows the time history of the aeroelastic responses of the panel and the NES at $\lambda = 355$. It can be seen that when the response amplitude of the panel reaches a specific value, the response amplitude of the NES increases abruptly, and the response amplitude of the panel then begins to decrease, which illustrates that the targeted energy transfer occurs. Here, the targeted energy transfer is achieved by recurrent transient resonance capture (TRC) [24]. The panel exhibits a series of recurrent motion finally. Figure 9(b) shows the time history of the responses of the panel and the NES at $\lambda = 368$. In the initial phase, the NES exhibits transient resonance capture as the same as Figure 8(b). When the response tends to be stable, the NES exhibits permanent resonance capture (PRC) [24], and the aeroelastic responses of the panel are permanently suppressed in a LCO with small amplitudes.

Figure 10 shows the time histories of the energy with an NES at $\lambda = 355$ and $\lambda = 368$. When the panel exhibits a series of recurrent motion, the vibration energy of the panel reaches a specific value, the energy dissipated by the damping of the panel, and NES increases rapidly, which illustrates that targeted energy transfer occurs and the NES pumps out vibration energy from the panel rapidly. Meanwhile, the aerodynamic load does negative work on the panel, which reduces the vibration energy of the panel. However, the energy of the panel has not reduced to zero, and the energy of the panel then increases owing to the input energy from the airflow. When the energy of the panel reaches the specific value, the NES will pump out energy from the panel again. This is a recurring cycle as shown in Figure 10(a), and the vibration response of the panel with an NES thus exhibits a series of recurrent motions, and the vibration amplitudes are limited to a smaller range. When the panel exhibits a LCO with small amplitudes, in the initial phase, the NES pumps out vibration energy from the panel the same as Figure 10(a); however, as time passes, the input energy from the airflow is gradually balanced with the dissipated energy by the damping as shown in Figure 10(b), and the panel reaches to a stable LCO motion with small amplitudes.

4.4. Region D. In region D, the response of the panel with or without an NES exhibits a stable LCO as shown in Figure 11(a) at $\lambda = 370$. Although the response amplitude of the panel with an NES is smaller than that without an NES, the suppression effect of the NES on panel flutter is not as good as that in region C. It is hoped that the NES suppresses the response amplitude of the panel by transient resonance

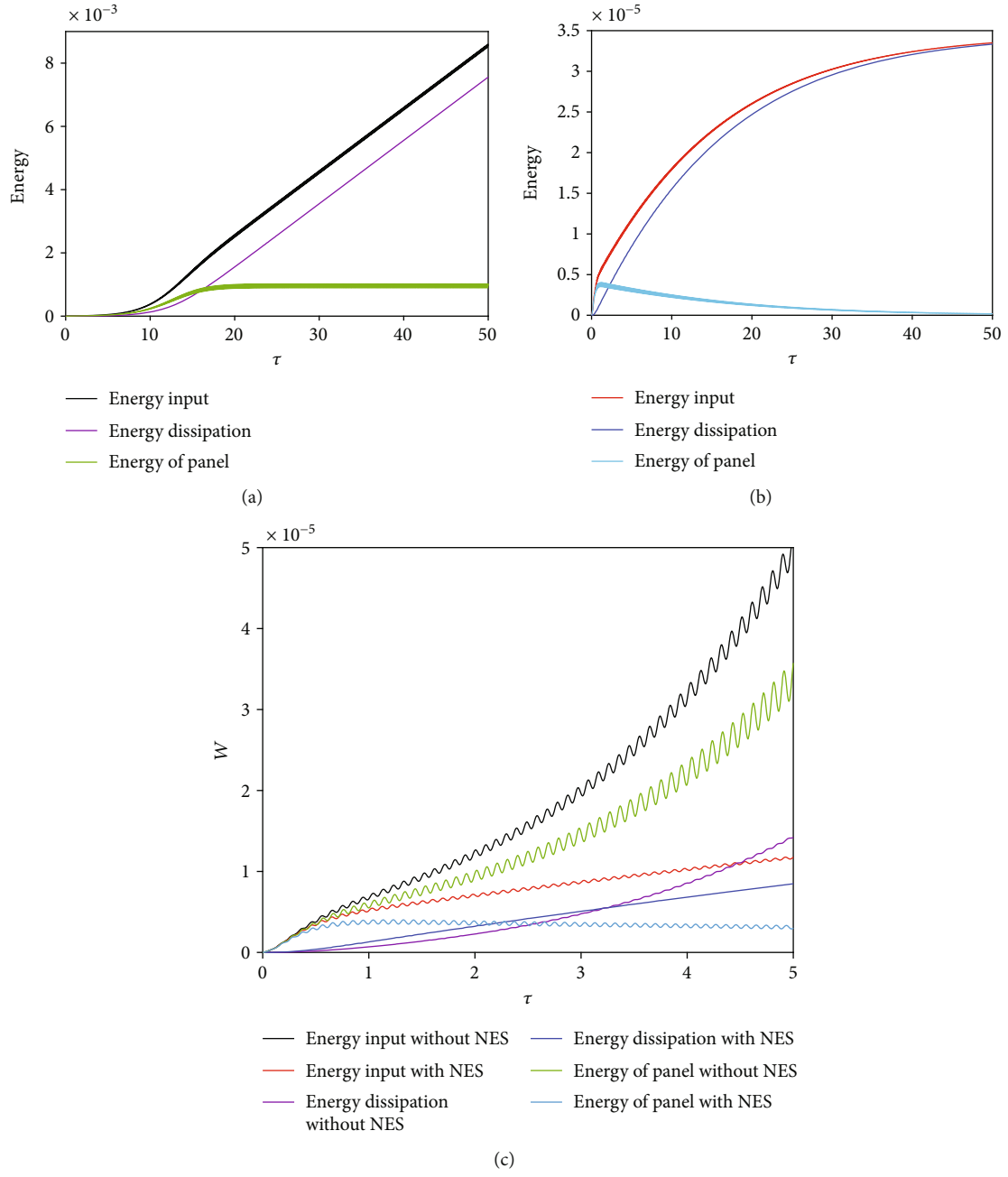

Figure 7: Time history of energy: (a) without an NES, (b) with an NES, and (c) comparisons in time 0-5.

capture in the initial phase in Figure 11(b); however, the NES is not sufficiently strong to reduce the response amplitude of the panel and only slows the increase in the response amplitude of the panel. The energy time history with an NES is similar to that without NES. The difference between the energy input by the airflow and energy dissipated by the damping of the panel and NES increases steadily with time and eventually reaches a balance (not zero). The panel finally exhibits a stable LCO. Although the NES cannot suppress the panel response as effectively as it does in region C, the total input energy provided by the airflow is reduced substantially, such as in Figure 12.

5. Effects of NES Parameters

The ability of the NES to suppress panel flutter depends on the values of its parameters. The dependence is assessed by determining the amplitudes of the panel response for different installation positions $\bar{d}$, masses M_{nes}, stiffness coefficients K_{nes}, and damping coefficients C_{nes} of the NES. The four baseline parameters of the NES are $M_{\text{nes}} = 0.03$, $K_{\text{nes}} = 80000$, $C_{\text{nes}} = 0.2$, and $\bar{d} = 0.55$. In the study on the effect of one specific parameter of the NES, the value of this parameter is changed to examine the aeroelastic response of the panel while the other three parameters are fixed. The

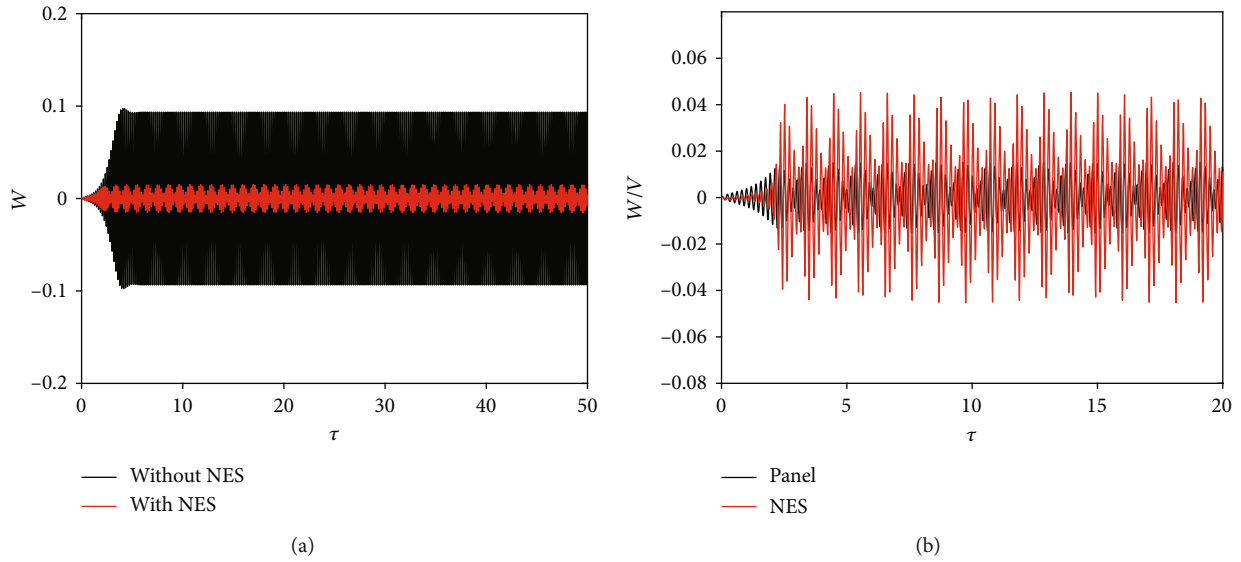

Figure 8: Time history at $\lambda = 355$: (a) responses of the panel with and without an NES; (b) responses of the NES and panel.

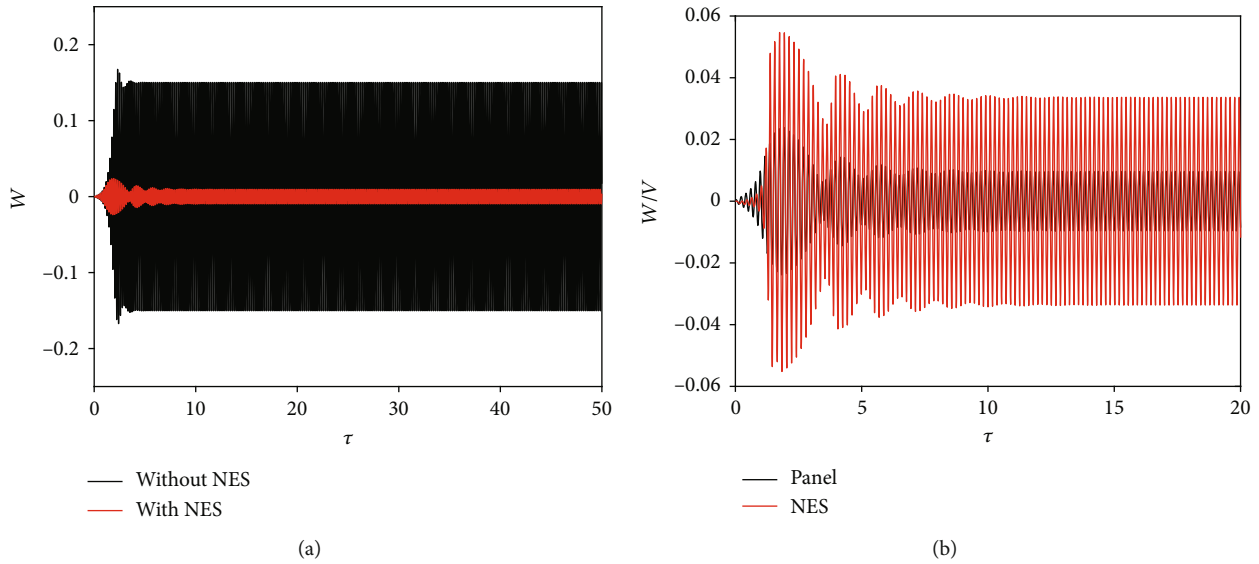

Figure 9: Time history at $\lambda = 368$: (a) responses of the panel with and without an NES; (b) responses of the NES and panel.

results presented in Figure 13 are obtained for $\lambda = 360$, and the response amplitude of the panel without an NES is 0.12. Figure 13(a) shows that the suppression effect of the NES on panel flutter differs when the NES is installed at different positions on the panel. The most effective installation position of the NES is near, but behind the center of the panel along the airflow direction, which indicates that the installation position of the NES depends on the direction of the airflow. Figure 13(b) shows the effect of the mass on the flutter response of the panel. It is seen that the responses of the panel are suppressed effectively when the mass is larger than 0.02; however, it is not that the higher the mass is, the better the suppression effect of the NES is. Figure 13(c) shows that the responses of the panel are not suppressed effectively when the nonlinear stiffness coefficient of the NES is too small or too large. And Figure 13(d) shows that the damping of the NES mainly affects the nonlinear aeroelastic behavior of the panel in the condition of $M_{\text{nes}} = 0.03$, $K_{\text{nes}} = 80000$, and $\bar{d} = 0.55$. Therefore, parameters of the NES must be carefully designed when the NES is applied to suppress the panel flutter response.

A design method for NES parameters is proposed to find a suitable combination of parameters of the NES. It is first necessary to determine the expected dynamic pressure. When the dynamic pressure is lower than this specific value, the NES can effectively control the aeroelastic response of the panel. In the present case, the expected dynamic pressure is set at $\lambda = 370$. Next, the installation position of the NES attached to the panel should be determined. According to the effect of the installation position discussed above, an

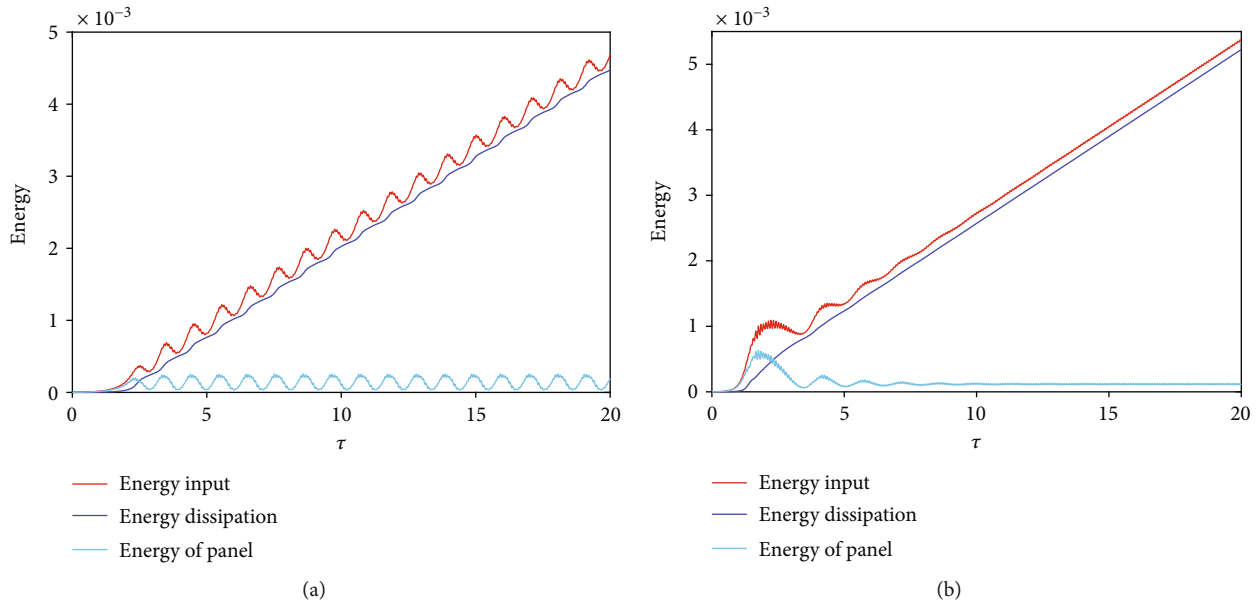

Figure 10: Time history of energy with an NES: (a) $\lambda = 355$; (b) $\lambda = 368$.

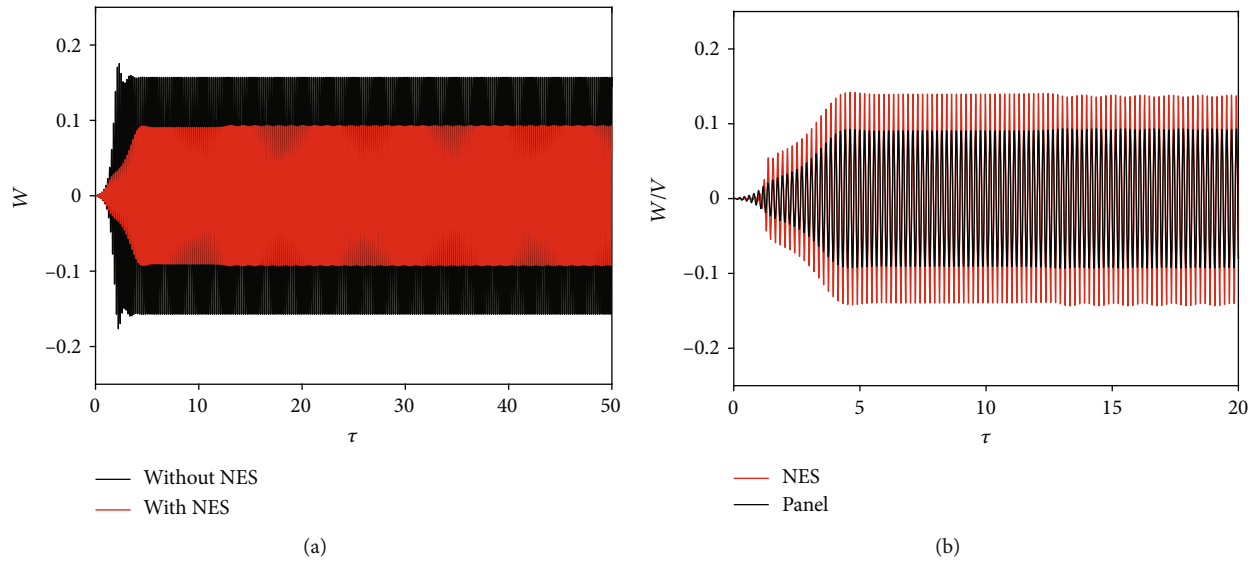

Figure 11: Time history at $\lambda = 370$: (a) responses of the panel with and without an NES; (b) responses of the NES and panel.

installation position behind the center of the panel along the airflow direction is preferable. In the present case, the NES is installed on the panel at the position $\bar{d} = 0.55$. Then, for different masses, maximum amplitude diagrams of the steady-state response of the panel are obtained by combining different damping and stiffness parameters, as shown in Figure 14. Assume that the expected response amplitude at $\lambda = 370$ is $W_{\max} \leq 0.023$, which is 15% of the maximum amplitude of the panel flutter response without an NES at $\lambda = 370$. In the present case, the masses are designed as 0.01, 0.02, 0.03, and 0.04, which are generally less than 0.1. When the masses of the NES are 0.01 and 0.02 in Figures 14(a) and 14(b), the minimum amplitude values of the steady-state amplitude responses of the panel are, respectively, 0.11 and 0.057, which show that the aeroelastic responses of the panel have not been suppressed effectively. When the masses of the NES is 0.03 in Figure 14(c), the minimum amplitude value is 0.018, which meets the design requirements. However, the minimum value is reached at only one peak, and when the damping and nonlinear stiffness coefficient changes, the amplitude value of the panel response changes dramatically. This indicates that there is no robust solution under these conditions. When the mass ratio of the NES is 0.04 in Figure 14(d), the minimum value of the steady-state amplitude response of the panel flutter is 0.00053. In addition, there is a flat area where the response of the panel is suppressed to smaller values. We can effectively select any set of parameters in this area; these will also meet the design requirements and have good robustness. Figure 15 is a bifurcation diagram with variations of dynamic pressure obtained in the condition of $M_{\text{nes}} = 0.04$, $C_{\text{nes}} = 0.5$, and

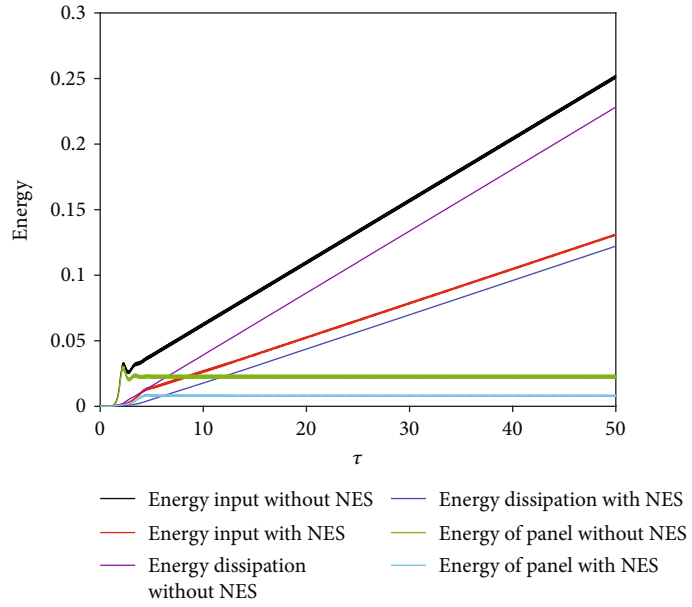

Figure 12: Time history of vibration energy.

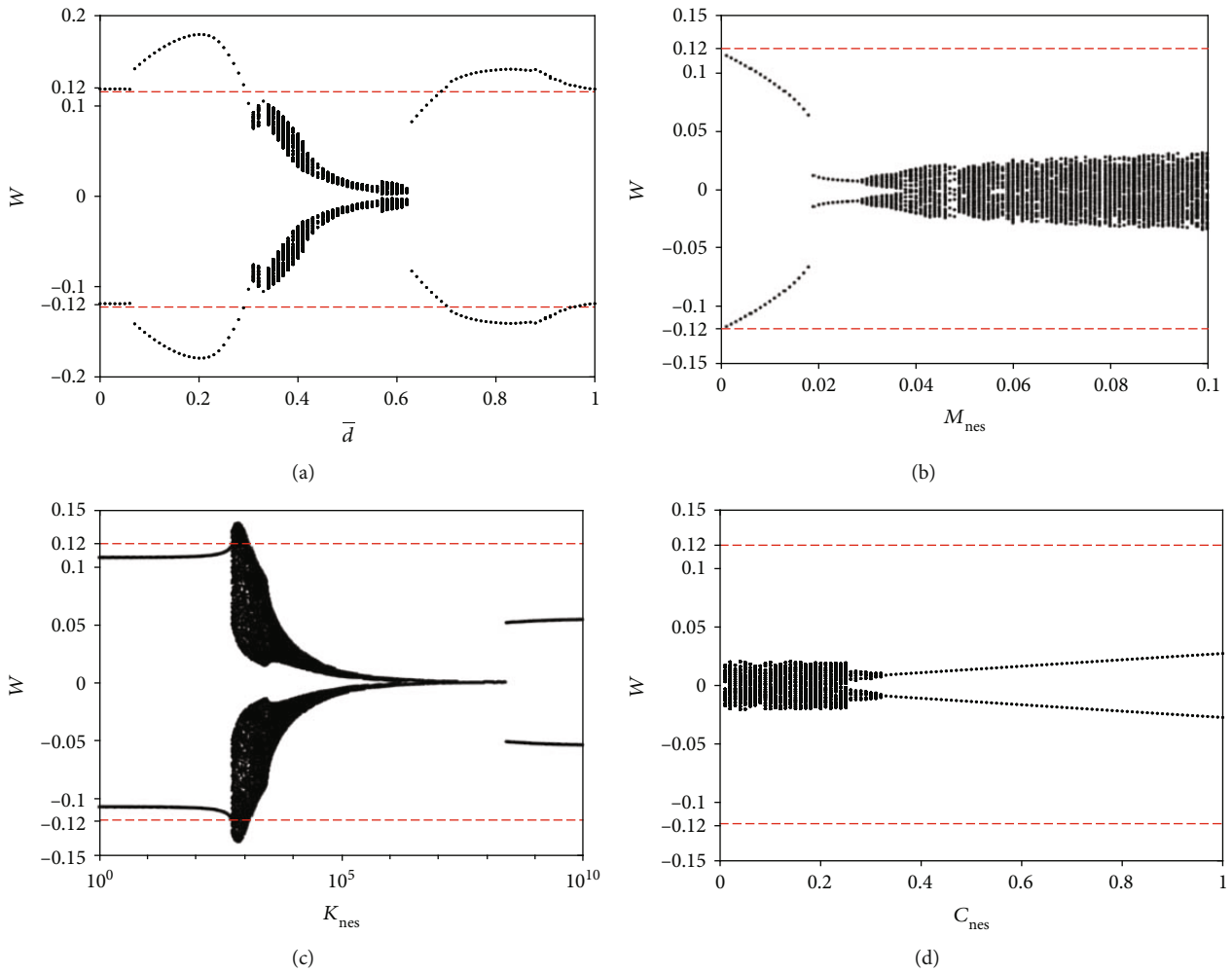

Figure 13: Bifurcation diagrams for different NES parameters: (a) location, (b) mass, (c) stiffness, and (d) damping.

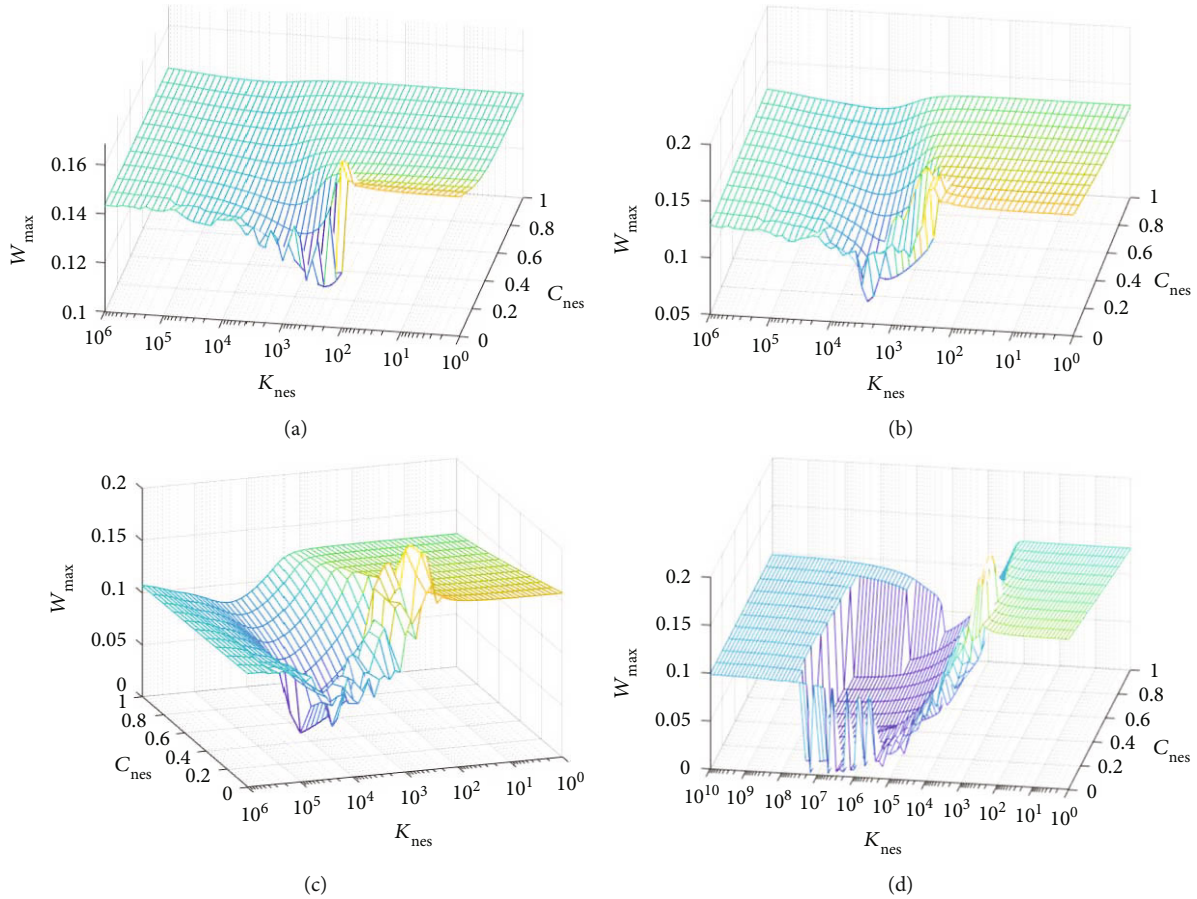

Figure 14: Effects of stiffness and damping coefficients for different masses: (a) 0.01, (b) 0.02, (c) 0.03, and (d) 0.04.

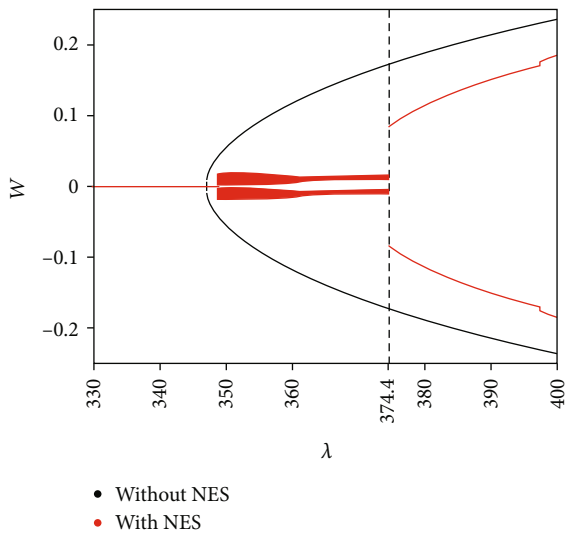

Figure 15: Bifurcation diagram in the condition of designed parameters.

$K_{nes} = 100000$. The maximum value of the steady-state amplitude response of the panel flutter is 0.012 at $\lambda = 370$. The figure illustrates the effectiveness of the proposed design method for NES parameters.

6. Conclusions

The mechanism of panel flutter suppression using an NES is explored. The following conclusions are drawn from the study:

(1) Parameters of the NES besides the nonlinear stiffness coefficient can increase or reduce the stability boundaries of the panel, but the effects are small

(2) The effect of the NES on the aeroelastic response of the panel can be described using a bifurcation diagram with respect to dynamic pressure. The diagram can be divided into four regions. In region A, the response of the panel with or without NES converges to its equilibrium position; however, the NES can drive the panel to the equilibrium position more rapidly. In region B, the response of the panel without NES exhibits a stable LCO, whereas the response of the panel with NES converges to its equilibrium position. In region C, the responses of the panel with NES are completely suppressed effectively by resonance capture of the NES. In region D, the response of the panel with or without NES exhibits a stable LCO, and the NES cannot suppress the panel response as effectively as it does in region C

(3) The most effective installation position of the NES is near, but behind the center of the panel along the airflow direction, it indicates that the installation position of the NES depends on the direction of the airflow

(4) A design method for the NES parameters is proposed to find a suitable combination of NES parameters that suppress the panel flutter effectively under the expected dynamic pressure, and both the design requirements and the robust characteristics should be considered

Data Availability

The data used to support the findings of this study are available from the corresponding author upon request.

Conflicts of Interest

We declare that we have no conflict of interest.

Acknowledgments

This study was funded by National Natural Foundation of China (Grant Nos. 11702204 and 11872050) and China Postdoctoral Science Foundation (Grant No. 2019M653585).

References

[1] I. E. Garrick and W. H. Reed Iii, "Historical development of aircraft flutter," *Journal of Aircraft*, vol. 18, no. 11, pp. 897–912, 1981.

[2] X. Zhou, L. Wang, J. Jiang, and Z. Su, "Hypersonic Aeroelastic Response of Elastic Boundary Panel Based on a Modified Fourier Series Method," *International Journal of Aerospace Engineering*, vol. 2019, Article ID 5164026, 13 pages, 2019.

[3] L. Q. Ye and Z. Y. Ye, "Effects of shock location on aeroelastic stability of flexible Panel," *AIAA Journal*, vol. 56, no. 9, pp. 3732–3744, 2018.

[4] P. Jin and X. Zhong, "Flutter Characteristic Study of Composite Sandwich Panel with Functionally Graded Foam Core," *International Journal of Aerospace Engineering*, vol. 2016, Article ID 7971435, 19 pages, 2016.

[5] M. Amabili and F. Pellicano, "Multimode Approach to Nonlinear Supersonic Flutter of Imperfect Circular Cylindrical Shells," *Journal of Applied Mechanics*, vol. 69, no. 2, pp. 117–129, 2002.

[6] E. H. Dowell, "Panel flutter - a review of the aeroelastic stability of plates and shells," *AIAA Journal*, vol. 8, no. 3, pp. 385–399, 1970.

[7] O. Seresta, M. M. Abdalla, S. B. Mulani, and P. Marzocca, "Stacking Sequence Design of Flat Composite Panel for Flutter and Thermal Buckling," *AIAA Journal*, vol. 44, no. 11, pp. 2726–2735, 2006.

[8] S. Panda and M. C. Ray, "Active control of geometrically nonlinear vibrations of functionally graded laminated composite plates using piezoelectric fiber reinforced composites," *Journal of Sound and Vibration*, vol. 325, no. 1-2, pp. 186–205, 2009.

[9] A. G. Cunha-Filho, A. M. G. de Lima, M. V. Donadon, and L. S. Leão, "Flutter suppression of plates using passive constrained viscoelastic layers," *Mechanical Systems and Signal Processing*, vol. 79, pp. 99–111, 2016.

[10] C. Shao, D. Cao, Y. Xu, and H. Zhao, "Flutter and Thermal Buckling Analysis for Composite Laminated Panel Embedded with Shape Memory Alloy Wires in Supersonic Flow," *International Journal of Aerospace Engineering*, vol. 2016, Article ID 856271, 12 pages, 2016.

[11] J. Zhou, M. Xu, and Z. Yang, "Aeroelastic stability analysis of curved composite panels with embedded Macro Fiber Composite actuators," *Composite Structures*, vol. 208, pp. 725–734, 2019.

[12] O. Gendelman, L. I. Manevitch, A. F. Vakakis, and R. M'Closkey, "Energy pumping in nonlinear mechanical oscillators: part I—dynamics of the underlying Hamiltonian systems," *Journal of Applied Mechanics*, vol. 68, no. 1, pp. 34–41, 2001.

[13] P. Malatkar and A. H. Nayfeh, "Steady-State dynamics of a linear structure weakly coupled to an essentially nonlinear oscillator," *Nonlinear Dynamics*, vol. 47, no. 1-3, pp. 167–179, 2006.

[14] M. Kurt, I. Slavkin, M. Eriten et al., "Effect of 1:3 resonance on the steady-state dynamics of a forced strongly nonlinear oscillator with a linear light attachment," *Archive of Applied Mechanics*, vol. 84, no. 8, pp. 1189–1203, 2014.

[15] X. Kong, H. Li, and C. Wu, "Dynamics of 1-dof and 2-dof energy sink with geometrically nonlinear damping: application to vibration suppression," *Nonlinear Dynamics*, vol. 91, no. 1, pp. 733–754, 2018.

[16] G. Gatti, "Fundamental insight on the performance of a nonlinear tuned mass damper," *Meccanica*, vol. 53, no. 1-2, pp. 111–123, 2018.

[17] F. Georgiades and A. F. Vakakis, "Dynamics of a linear beam with an attached local nonlinear energy sink," *Communications in Nonlinear Science and Numerical Simulation*, vol. 12, no. 5, pp. 643–651, 2007.

[18] P. Panagopoulos, F. Georgiades, S. Tsakirtzis, A. F. Vakakis, and L. A. Bergman, "Multi-scaled analysis of the damped dynamics of an elastic rod with an essentially nonlinear end attachment," *International Journal of Solids and Structures*, vol. 44, no. 18-19, pp. 6256–6278, 2007.

[19] M. Kani, S. E. Khadem, M. H. Pashaei, and M. Dardel, "Vibration control of a nonlinear beam with a nonlinear energy sink," *Nonlinear Dynamics*, vol. 83, no. 1-2, pp. 1–22, 2016.

[20] J. E. Chen, W. He, W. Zhang, M. H. Yao, J. Liu, and M. Sun, "Vibration suppression and higher branch responses of beam with parallel nonlinear energy sinks," *Nonlinear Dynamics*, vol. 91, no. 2, pp. 885–904, 2018.

[21] F. Georgiades and A. F. Vakakis, "Passive targeted energy transfers and strong modal interactions in the dynamics of a thin plate with strongly nonlinear attachments," *International Journal of Solids and Structures*, vol. 46, no. 11-12, pp. 2330–2353, 2009.

[22] J. Chen, W. Zhang, M. Yao, J. Liu, and M. Sun, "Vibration reduction in truss core sandwich plate with internal nonlinear energy sink," *Composite Structures*, vol. 193, pp. 180–188, 2018.

[23] A. E. Mamaghani, S. E. Khadem, and S. Bab, "Vibration control of a pipe conveying fluid under external periodic excitation using a nonlinear energy sink," *Nonlinear Dynamics*, vol. 86, no. 3, pp. 1761–1795, 2016.

[24] Y. S. Lee, A. F. Vakakis, L. A. Bergman, D. M. McFarland, and G. Kerschen, "Suppression aeroelastic instability using broadband passive targeted energy transfers, part 1: theory," *AIAA Journal*, vol. 45, no. 3, pp. 693–711, 2007.

[25] Y. Bichiou, M. R. Hajj, and A. H. Nayfeh, "Effectiveness of a nonlinear energy sink in the control of an aeroelastic system," *Nonlinear Dynamics*, vol. 86, no. 4, pp. 2161–2177, 2016.

[26] N. Ebrahimzade, M. Dardel, and R. Shafaghat, "Performance comparison of linear and nonlinear vibration absorbers in aeroelastic characteristics of a wing model," *Nonlinear Dynamics*, vol. 86, no. 2, pp. 1075–1094, 2016.

[27] Z. Yan, S. A. Ragab, and M. R. Hajj, "Passive control of transonic flutter with a nonlinear energy sink," *Nonlinear Dynamics*, vol. 91, no. 1, pp. 577–590, 2018.

[28] W. Zhang, Y. Liu, S. Cao, J. Chen, Z. Zhang, and J. Zhang, "Targeted energy transfer between 2-D wing and nonlinear energy sinks and their dynamic behaviors," *Nonlinear Dynamics*, vol. 90, no. 3, pp. 1841–1850, 2017.

[29] Y. W. Zhang, H. Zhang, S. Hou, K. F. Xu, and L. Q. Chen, "Vibration suppression of composite laminated plate with nonlinear energy sink," *Acta Astronautica*, vol. 123, pp. 109–115, 2016.

[30] D. R. Q. Pacheco, F. D. Marques, and A. J. M. Ferreira, "Panel flutter suppression with nonlinear energy sinks: Numerical modeling and analysis," *International Journal of Non-Linear Mechanics*, vol. 106, pp. 108–114, 2018.

[31] E. H. Dowell, "Nonlinear oscillations of a fluttering plate," *AIAA Journal*, vol. 4, no. 7, pp. 1267–1275, 1966.

[32] F. Tong and P. Xue, *Vibration Theory and Application*, Northwestern Polytechnical University Press, Xi'an, China, 1998, (in Chinese).

[33] H. Krause and D. Dinkler, "The influence of curvature on supersonic panel flutter," in *39th AIAA/ASME/ASCE/AHS/ASC Structures, Structural Dynamics, and Materials Conference and Exhibit*, Long Beach,CA,U.S.A., 1998.

[34] R. Bellet, B. Cochelin, P. Herzog, and P.-O. Mattei, "Experimental study of targeted energy transfer from an acoustic system to a nonlinear membrane absorber," *Journal of Sound and Vibration*, vol. 329, no. 14, pp. 2768–2791, 2010.